Active Site of O_2 and Its Improvement Mechanism over Ce-Ti Catalyst for NH_3-SCR Reaction

Dong Jiang [ID]**, Shule Zhang *, Yiqing Zeng, Pengfei Wang and Qin Zhong ***

School of Chemical Engineering, Nanjing University of Science and Technology, Nanjing 210094, China; dongjiang304@163.com (D.J.); yiqingzeng@163.com (Y.Z.); Pengfeiwang99@163.com (P.W.)
* Correspondence: shulezhang@163.com (S.Z.); zq304@njust.edu.cn (Q.Z.);
  Tel.: +86-152-5099-6311 (S.Z.); +86-136-0519-9817 (Q.Z.)

Abstract: The current study on Ce-Ti catalyst was mainly focused on the function of NH_3 and NO adsorption sites. In our study, by comparing Ce-Ti (doped catalyst) to Ce/Ti (supported catalyst), the active site of O_2 and its improvement mechanism over Ce-Ti catalyst for NH_3-Selective catalytic reduction (SCR) reactions were investigated. For Ce-Ti catalyst, a cerium atom was confirmed entering a TiO_2 crystal lattice by X-ray diffraction (XRD) and Raman; the structure of Ce-□-Ti (□ represents oxygen vacancy) in Ce-Ti catalyst was confirmed by X-ray photoelectron spectroscopy (XPS) and Photoluminescence spectra (PL spectra). The nature of this structure was characterized by electron paramagnetic resonance (EPR), Ammonia temperature-programmed desorption (NH_3-TPD), hydrogen temperature-programmed reduction (H_2-TPR), Nitric oxide temperature-programmed desorption (NO-TPD) and In situ DRIFT. The results indicated that oxygen vacancies had a promotive effect on the adsorption and activation of oxygen, and oxygen was converted to superoxide ions in large quantities. Also, because of adsorption and activation of NO and NH_3, electrons were transferred to adsorbed oxygen via oxygen vacancies, which also promoted the formation of superoxide ions. We expected that our study could promote understanding of the active site of O_2 and its improvement mechanism for doped catalyst.

Keywords: Ce-Ti; NH_3-SCR; Ce-□-Ti; oxygen vacancies; superoxide ions

1. Introduction

NO_x (NO_2, NO, N_2O etc.) emitted from mobile or stationary sources causes a series of serious environmental problems such as ozone holes, photochemical smog and acid rain [1], which are harmful to human health. Selective catalytic reduction (SCR) is the mainstream technology that used for denitrification nowadays. V_2O_5-WO_3/TiO_2 catalysts are the most widely used industrial catalyst due to their good catalytic performance and excellent resistance to SO_2 [2]. However, there are some defects, such as a narrow temperature window, biological toxicity of V_2O_5, generation of larger amount of N_2O at high temperature, etc. [3]. CeO_2-based catalysts have been proved to possess excellent low-temperature activity for NH_3-SCR of NO due to their high oxygen storage capacities along with unique redox properties [4]. Among all these catalysts, Ce-Ti catalyst has gained wide attention for its excellent properties and lack of secondary pollution.

A lot of relevant work [5–7] on Ce-Ti catalyst have been performed. Gao et al. [8] yielded 98.6% NO conversion at around 350 °C with Ce-Ti mixed-oxide catalyst. They attributed the superior performance to the strong interaction between Ce and Ti. Moreover, they thought that high concentration of amorphous Ce on the surface played a vital role in NO reduction. Li et al. [9] studied amorphous Ce-Ti catalyst and put forward the important structure of Ce-O-Ti. In addition, the Ce-O-Ti structure with the interaction between Ce and Ti was confirmed to be the main active site. Li et al. [10] later reported

that NH_3 adsorption on Ti and NO adsorption on Ce played a key role in NH_3-SCR with Ce-Ti catalyst. Based on this, some researchers focused on the transition metal-modified Ce-Ti catalyst and gained good results [11,12]. However, little attention was paid to the mechanism of how oxygen participated in the SCR reaction in Ce-Ti catalyst.

In our present study, we also found that Ce-Ti catalyst showed a higher NH_3-SCR activity than Ce/Ti catalyst, especially in the low-temperature region. Based on previous studies, we focused on the structure of Ce-Ti catalyst, active site of O_2 and its improvement mechanism for NH_3-SCR reaction by a series of characterization include X-ray diffraction (XRD), PL, electron paramagnetic resonance (EPR), Raman, X-ray photoelectron spectroscopy (XPS), H_2-TPR, NO-TPD, NH_3-TPD, H_2-TPR and In situ DRIFT. We expected that our study could promote understanding of the active site of O_2 and its improvement mechanism for doped SCR catalyst.

2. Result and Discussion

2.1. Catalytic Activity Tests

Four kinds of catalysts, Ce-Ti-500, Ce-Ti-400, Ce/Ti-500 and Ce/Ti-400, were tested for NO conversion from 120 °C to 390 °C (Figure 1). As shown in Figure 1, the NO conversion mainly increased with the increase of reaction temperature (except Ce/Ti-500 at 400 °C). Among the four kinds of catalysts, the Ce-Ti-400 catalyst showed a superior SCR activity, especially at low temperatures (<300 °C). The NO conversion of Ce-Ti-400 could reach 59.1% and 85.8% at 210 and 240 °C, respectively, and little NO could be detected in outlet gas flow above 270 °C. These results were similar to traditional Ce-Ti catalysts [13,14]. Additionally, the formation of N_2O was <3 ppm, which means the N_2 selectivity was promising. It is worth noting that the NO conversion at low temperatures (<300 °C) increased in the following order: Ce/Ti-500 < Ce/Ti-400 < Ce-Ti-500 < Ce-Ti-400. Therefore, compared with the supported catalysts (Ce/Ti catalysts), the doped catalysts (Ce-Ti catalysts) showed higher NH_3-SCR activity.
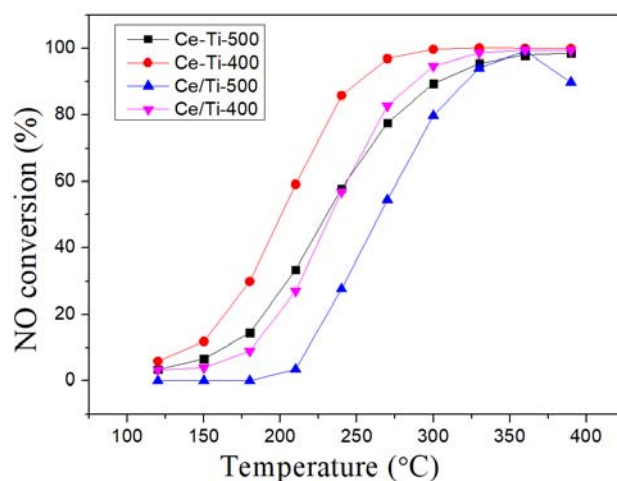

Figure 1. NO removal of Ce-Ti-500, Ce-Ti-400, Ce/Ti-500 and Ce/Ti-400 at different temperature.

2.2. XRD and Raman Analysis

Figure 2 displays the XRD patterns of catalysts prepared by different methods. As shown in Figure 2, Ce-Ti-400 and Ce-Ti-500 catalysts only showed the anatase type of TiO_2 (2θ = 25.2°, 37.7°, 47.8°, 53.8°, 55.0°). No representative peaks of Ce species were found. The doped catalyst (Ce-Ti-400) had lower XRD peak intensity than that of supported catalyst (Ce/Ti-400). According to a previous study on Ce-Ti catalyst [15], the anatase peak intensity of catalysts decreased with the increase in Ce doping level, suggesting that Ce interacted with Ti. For Ce-Ti-500, only anatase was detected.

However, large amounts of rutile were detected in Ce/Ti-500. As we know, Ce doping could inhibit phase transformation from anatase to rutile [16], which could be an evidence of Ce doped into the TiO_2 lattice for Ce-Ti-400 catalyst. Energy Dispersive Spectroscopy (EDS) results showed that the cerium ratio on the surface of Ce-Ti-400 catalyst was 5.98%, while that of Ce/Ti-400 was 10.29%. The above data could also prove that Ce had entered TiO_2 lattice. In addition, TiO_2 (anatase) is considered to be the best supporter of SCR catalysts because it improves dispersion and reducibility of rhodium particles [17].
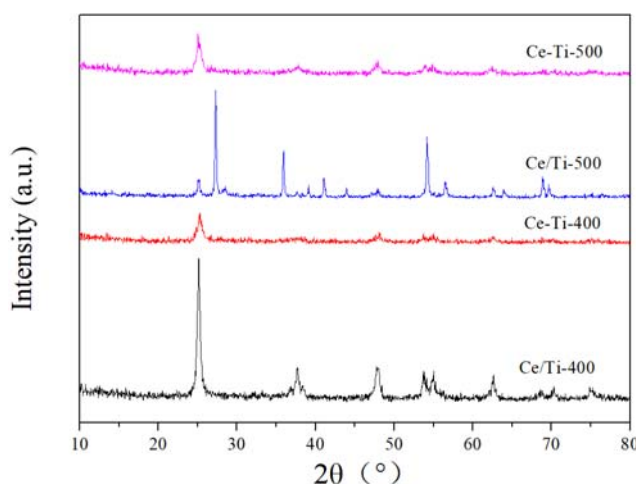
Figure 2. X-ray diffraction (XRD) patterns of catalysts prepared by different methods.

The Raman spectra were used to investigate the structure of samples further. Raman spectra of Ce-Ti-400 and Ce/Ti-400 are showed in Figure 3. Referring to the standard Raman spectrum, the peaks at 640 cm^{-1}, 515 cm^{-1}, 398 cm^{-1}, 198 cm^{-1} and 147 cm^{-1} are representative peaks of anatase TiO_2. The anatase bands at 515 and 398 cm^{-1} could be attributed to the Ti-O-stretching vibration, and the bands at 640 cm^{-1} could be attributed to O-Ti-O-bending vibrations [18,19]. Obviously, the Raman spectra of Ce/Ti-400 coincides with the standard anatase TiO_2 Raman spectrum well. However, in the Raman spectra of Ce-Ti-400, only a weak peak at 144 cm^{-1} could be found. This phenomenon showed that the original symmetrical structure of Ti-O-Ti was destroyed by Ce doping. Thus, we could infer that in Ce-Ti-400 sample, the new structure of Ce-O-Ti formed [9].
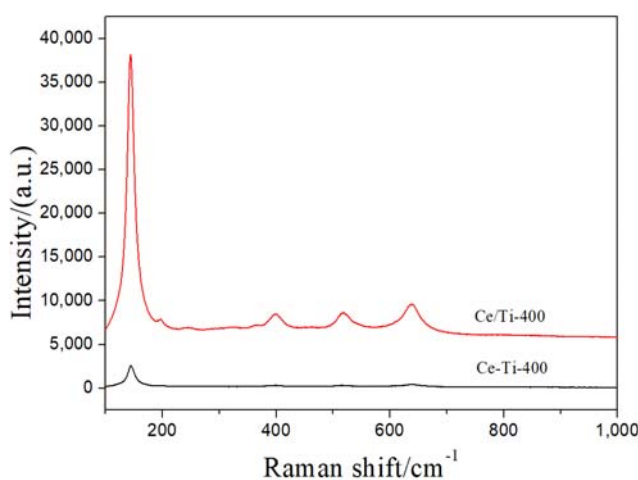
Figure 3. Raman spectra of Ce-Ti-400 and Ce/Ti-400.

2.3. XPS and PL Analysis

Figure [4] shows XPS spectrum for Ce3d, Ti2p and O1s of Ce-Ti 400 and Ce/Ti 400. From the XPS spectrum of Ce 3d in Figure [4]a, two multipliers (U and V) could be found after fitting. The XPS peaks labeled U, U″, U‴, V, V″, and V‴ were attributed to Ce^{4+} species, while the u′, v′ peaks were assigned to Ce^{3+} species. Compared to Ce/Ti-400, it could be clearly seen that peaks of Ce-Ti-400 slightly shifted to lower binding energy. As we know, lower binding energy means higher cloud density [20]. This change corresponded with previous inference of Ce-O-Ti structure. By calculation, the amount of $Ce^{3+}/(Ce^{3+} + Ce^{4+})$ of Ce-Ti-400 and Ce/Ti-400 were 32.63% and 19.11%, respectively. Obviously, Ce-Ti-400 has a higher amount of $Ce^{3+}/(Ce^{3+} + Ce^{4+})$. It could be inferred that the interaction between Ce and Ti promote the increase of Ce^{3+}. The increase of Ce^{3+} could bring more oxygen vacancies, which is beneficial to activity enhancement [21].
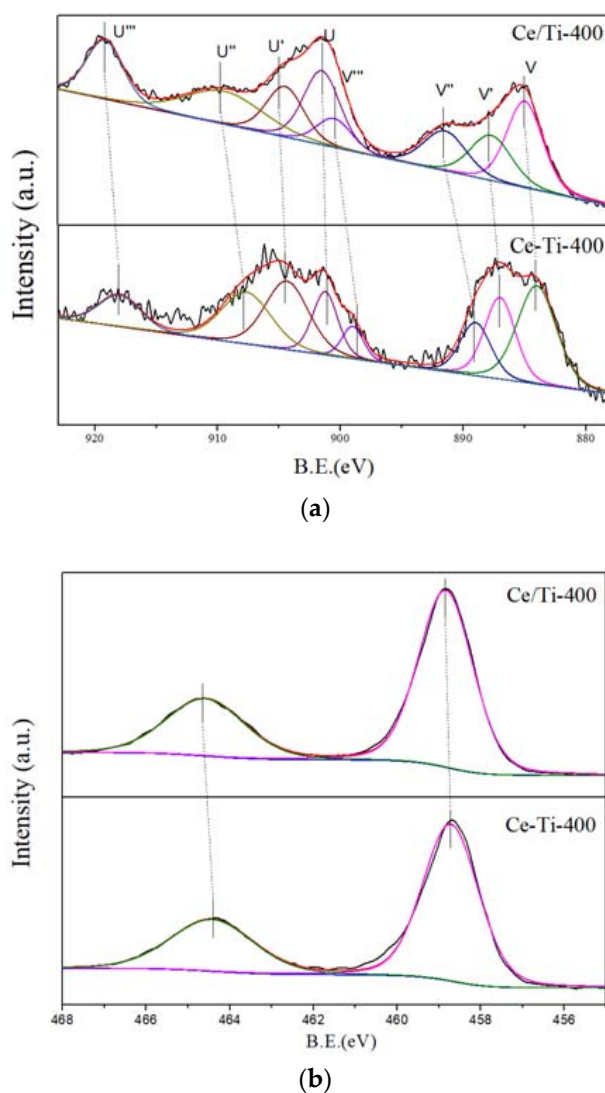

(a)

(b)

Figure 4. *Cont.*
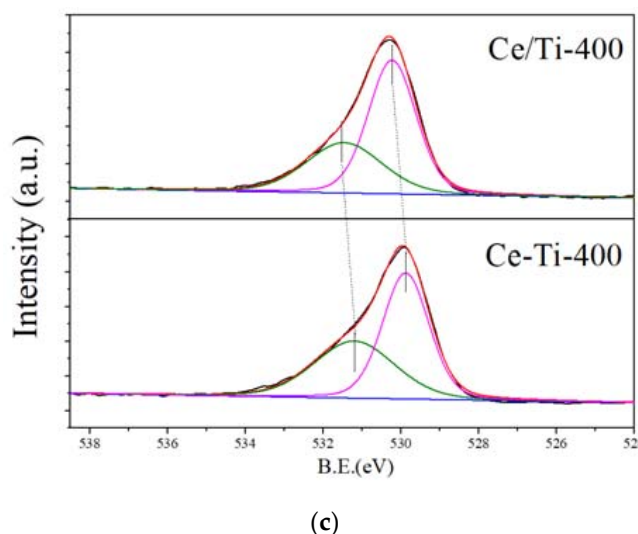
(**c**)

Figure 4. XPS results of Ce 3d (**a**), Ti 2p (**b**) and O 1s (**c**).

Figure 4b shows the XPS spectrum of Ti2p of Ce-Ti-400 and Ce/Ti-400. The main peaks at 455.8–461.4eV and 462.3–467.2 eV could be assigned to Ti^{4+} [22]. Obviously, cloud density of both Ce and Ti increased. Through previous result of Raman, we confirmed the structure of Ce-O-Ti in Ce-Ti-400 sample. Normally, due to the different electronegativity of Ce ion and Ti ion, the density of Ce and Ti cloud density could not increase at the same time in Ce-O-Ti structure. Therefore, combined with the increasing cloud density of both Ce and Ti, we could infer that for fresh catalysts, oxygen vacancies existed in Ce-O-Ti structure. Thus, Ce-□-Ti possibly existed in Ce-Ti-400 catalyst.

Figure 4c shows the XPS spectrum of O 1s of Ce-Ti-400 and Ce/Ti-400. The two kinds of peaks in these spectra represented two kinds of surface oxygen species. Normally, the peak at 531.0–531.9eV with lower binding energy could be assigned to lattice oxygen (denoted as O_β), and the peak 529.0–530.0 eV with higher binding energy could be assigned to chemisorbed oxygen (denoted as O_α) [23,24]. It is worth noting that peaks of Ce-Ti-400 slightly shifted to lower binding energy and this result means O of Ce-Ti-400 also has higher cloud density. Normally, oxygen vacancy was charged oxygen vacancy [25]. In addition, combined with the increasing cloud density of both Ce and Ti in this study, it could also be judged that oxygen vacancy was charged oxygen vacancy. Considering the strong electron absorption ability of O and adsorbed oxygen on catalysts, it is possible that electrons on the oxygen vacancy will produce a certain amount of delocalization, which led to the increase of cloud intensity of O_α and O_β on catalyst.

Figure 5 shows PL spectrum of Ce-Ti-400 and Ce/Ti-400. From previous report, peak 1 at 556 nm was assigned to the surface defect, peak 2 at 633 nm might be attributed to the transfer of excited electrons [26,27]. Obviously, the intensity of Ce-Ti-400 was lower than that of Ce/Ti-400. As we have shown, surface defects were electron-trapping centers in catalysts. In addition, a lower PL intensity represented a larger number of surface defects in general [28]. Oxygen vacancy was the main surface defect for these two catalysts. That means more oxygen vacancies existed on Ce-Ti-400. From our previous study [22], formation of oxygen vacancies was due to the interaction between doping Ce and Ti. On the one hand, the formation of oxygen vacancies could promote low-temperature SCR activity [29]; on the other hand, oxygen vacancies were the adsorption center of oxygen [30]. The absorbed oxygen could be transformed to superoxide ions, which were important active species for the SCR reaction. The analysis of above-mentioned aspects with the influence of NH_3 and NO to oxygen vacancies would be the key to the effect of oxygen vacancies on denitrification at low temperature. Further study of the above issues are carried out in this paper.
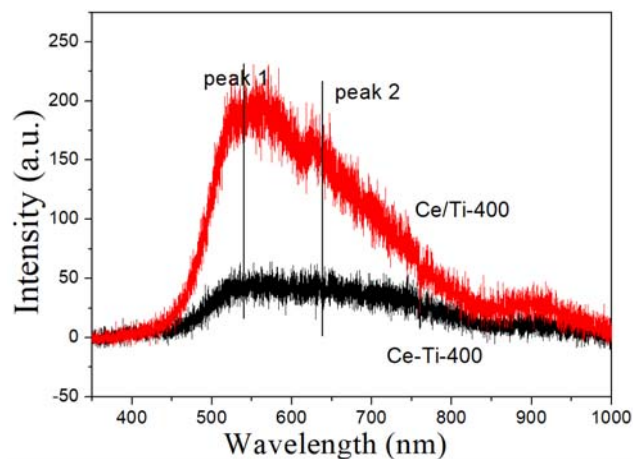
Figure 5. PL spectrum of Ce-Ti-400 and Ce/Ti-400.

2.4. NO-TPD and NH₃-TPD

NO-TPD experiments were carried out to investigate the NO adsorption/desorption active sites and behaviors. Figure 6 showed the NO-TPD results of Ce-Ti-400 and Ce/Ti-400. From Figure 6, the curve of TiO_2 did not show any consumption peak of NO. However, CeO_2 showed two peaks centered at the tempura range from 200 to 300 °C (Peak I) and from 300 to 400 °C (Peak II). For Ce-Ti-400 and Ce/Ti-400, Peak I and Peak II were detected at similar temperature range. Also, Ce-Ti-400 and Ce/Ti-400 had similar peak intensity ratio to CeO_2. It could be inferred that Ce sites might be the main adsorption site to NO for Ce-Ti-400 and Ce/Ti-400. It is worth noting that Peak I and Peak II of Ce-Ti-400 had higher peak intensity than those of Ce/Ti-400. The NO-TPD peaks above 150 °C are due to the decomposition of relatively thermal stable nitrate, such as bidentate nitrate [31]. The formation of nitrate species is essential in the process of NH₃-SCR reaction. It has been confirmed that nitrate species could significantly improve the low-temperature SCR activity [32]. Therefore, Ce-Ti-400 catalyst has better oxidation effect on NO and promoted denitrification at low temperature. EDS analysis results (Figures S3 and S4) show that more cerium exists on the surface of Ce/Ti-400 than on Ce-Ti-400. The amount of cerium (Ce sites) on the surface of catalyst is not the reason for the increase of NO oxidation.
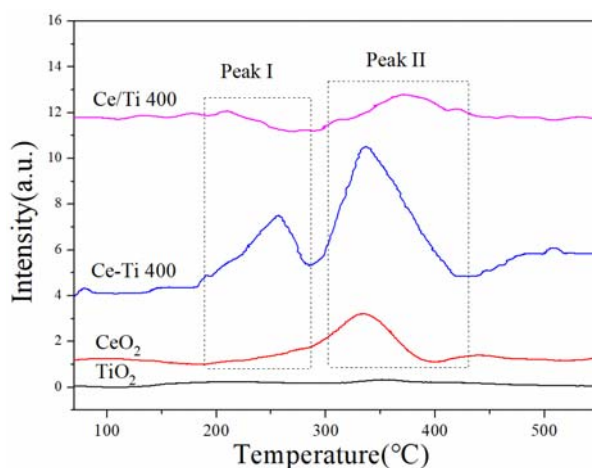

Figure 6. NO-TPD profiles of Ce-Ti-400 and Ce/Ti-400.

Figure 7 showed the ammonia desorption results of Ce-Ti-400 and Ce/Ti-400. The different acidic sites, including both Brønsted and Lewis acidic sites, could be investigated by NH₃-TPD [33].

In the experimental temperature range, for the CeO_2 sample, one NH_3-TPD peak for weak acidic sites between about 170 to 300 °C was observed. For Ce/Ti-400 catalyst, one NH_3-TPD peak for strong acidic sites between about 300 to 500 °C was observed. Both strong and weak peaks could be detected on the NH_3-TPD curve of TiO_2 sample. Therefore, Ti sites might be the acidic sites in Ce-Ti-400. Li [10] drew the same conclusion that TiO_2 plays the role in providing surface Lewis acid sites. One may argue that weak NH_3 desorption peak on Ce-Ti-400 was similar to that of CeO_2. It is worth noting that no desorption peak similar to CeO_2 was detected on the curve of Ce/Ti-400. Therefore, Ce sites were not adsorption sites of NH_3. From calculation of the peak area, a larger area of Ce-Ti-400 means more acidic sites existed in Ce-Ti-400 than Ce/Ti-400. More acidic sites were favorable for the adsorption of NH_3 and considered to improve the SCR reaction [3].
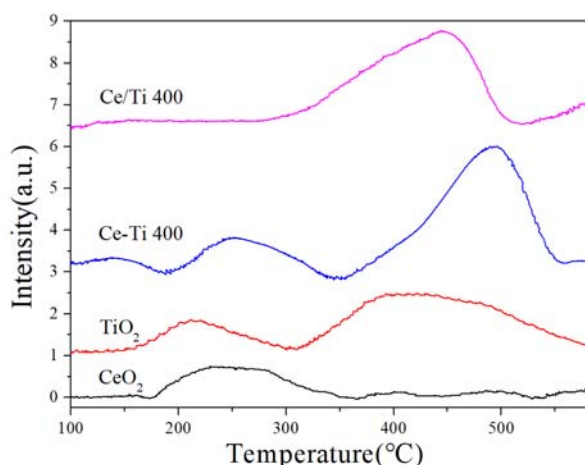

Figure 7. NH_3-TPD profiles of Ce-Ti-400 and Ce/Ti-400.

2.5. H2-TPR and EPR Analysis

H_2-TPR is widely used in evaluating the redox capacity of SCR catalyst. In our experiment, we used $5\%O_2$ + $95\%N_2$ to treat the sample for 2h and detected H_2-TPR signal. Figure 8 showed the H_2-TPR profiles of Ce-Ti-400 and Ce/Ti-400. TiO_2 had no obvious H_2 consumption peaks in the curve. Different from the curve of TiO_2, CeO_2 showed two peaks centered at about 450 °C and 550 °C. Therefore, Ti sites were not the redox center of this reaction. Redox center of the catalyst was related to Ce sites. For Ce-Ti-400, two weak peaks located at 255 °C and 393 °C were likely assigned to the reduction of surface oxygen [34]. The third peak located at 614 °C could be assigned to the reduction of Ce^{4+} to Ce^{3+} [35,36]. Considering that chemisorbed oxygen was easily oxidized, the first peak for Ce-Ti-400 might relate to chemisorbed oxygen, and the second peak might relate to surface active lattice oxygen. For Ce/Ti-400, three peaks appeared in a similar position as Ce-Ti-400. In our test, molar weight of Ce for CeO_2 was 0.00058mol, for Ce-Ti-400 and Ce/Ti-400 was 0.00012 mol. In other words, Ce species of Ce-Ti-400 and Ce/Ti-400 were four fifths less than that of CeO_2. However, the peak area of Ce-Ti-400 and Ce/Ti-400 was larger than that of CeO_2. Thus, the interaction of Ce and Ti could significantly improve redox of catalyst. Compared with Ce/Ti-400, the first two peaks of Ce-Ti-400, which represented surface oxygen, was larger than Ce/Ti-400. Combined with the activity of catalysts and discussion above, the first peak showed that the structure of Ce-□-Ti had a stronger ability to adsorb and activate oxygen; the second peak showed that surface active lattice oxygen was more active, i.e., oxygen vacancies were easier to form in Ce-Ti catalyst due to the Ce-O-Ti structure. Oxygen vacancies of SCR catalysts could affect its performance of store and release superoxide ions, which was important for the NO removal [37]. In low-temperature denitrification, superoxide ions were quite important because they could oxidize NO and promote low-temperature SCR reaction. Therefore, EPR spectra were used to further research properties of superoxide ions.
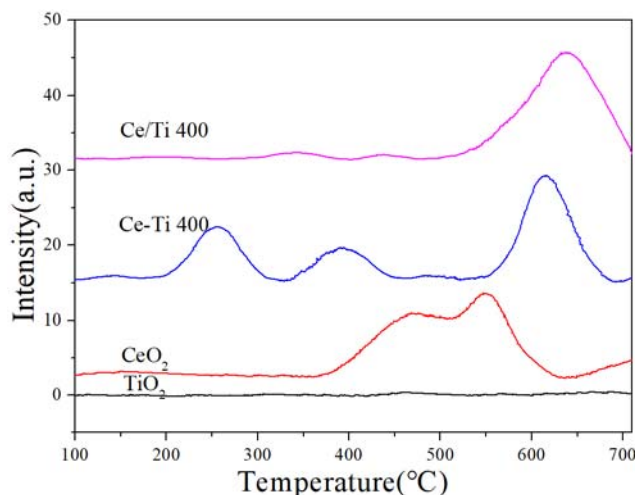
Figure 8. H_2-TPR profiles of Ce-Ti-400 and Ce/Ti-400.

Figure 9 shows EPR spectra profiles of Ce/Ti-400 and Ce-Ti-400. In our experiment, we used different gases to treat the sample for 2h and detected EPR signal. The signals at g = 2.0036 was attributed to the superoxide ions [38]. Compared to Ce-Ti-400 (Figure 9b), EPR intensity of Ce/Ti-400 (Figure 9a) shows little change when atmosphere changed, and peak intensity was much lower. It suggests that very few superoxide ions existed in the sample Ce/Ti-400, and there are obviously more superoxide ions in Ce-Ti-400 catalyst. As confirmed above, the structural differences between Ce-Ti-400 and Ce/Ti-400 are mainly reflected in the Ce-O-Ti (Ce-□-Ti) structure in Ce-Ti-400. Therefore, we could draw the following conclusions: for doped Ce-Ti catalyst, the Ce site was the active site of NO adsorption and Ti site was the active site of NH_3 adsorption, and oxygen vacancy was the active site of O_2 adsorption in the structure of Ce-□-Ti. There have been a lot of papers about the activation of NO and NH_3 [39–41]. However, regarding how chemisorbed oxygen was activated, most of these papers stayed at the increase of chemisorbed oxygen and superoxide ions. No study regarding the change of activated oxygen in the atmosphere of NH_3 and NO on Ce-Ti catalyst has yet been reported.

As shown in Figure 9b, the intensity of superoxide ions decreased as O_2 + NO > NO + O_2 + NH_3 > O_2 + NH_3 > O_2. A small number of superoxide ions were observed when only O_2 was injected. It indicated that when only O_2 existed, the formation of superoxide ions was limited. For the NH_3 + O_2 test, the peak of superoxide ions increased clearly. During the process of activation of NH_3 adsorption to NH_2 in SCR reaction, electron transfer existed [42]. In addition, NH_3 species were electron-donating groups and able to donate electrons to oxygen vacancies [43,44]. In the structure of Ce-□-Ti, oxygen was adsorbed on the oxygen vacancies, which promoted the increase of active site electronegativity. Combined with EPR test results, it could be determined that electrons from NH_3 were transferred to O_2 finally and superoxide ions were produced. It is worth noting that TiO_2 showed little SCR activity and produced little superoxide ions. From the result of NH_3-TPD, a considerable amount of adsorption sites of NH_3 exist on TiO_2. Considering few oxygen vacancies on TiO_2 and denitrification activity of Ce-Ti-400, we could infer that oxygen vacancies were important to the activation of NH_3.
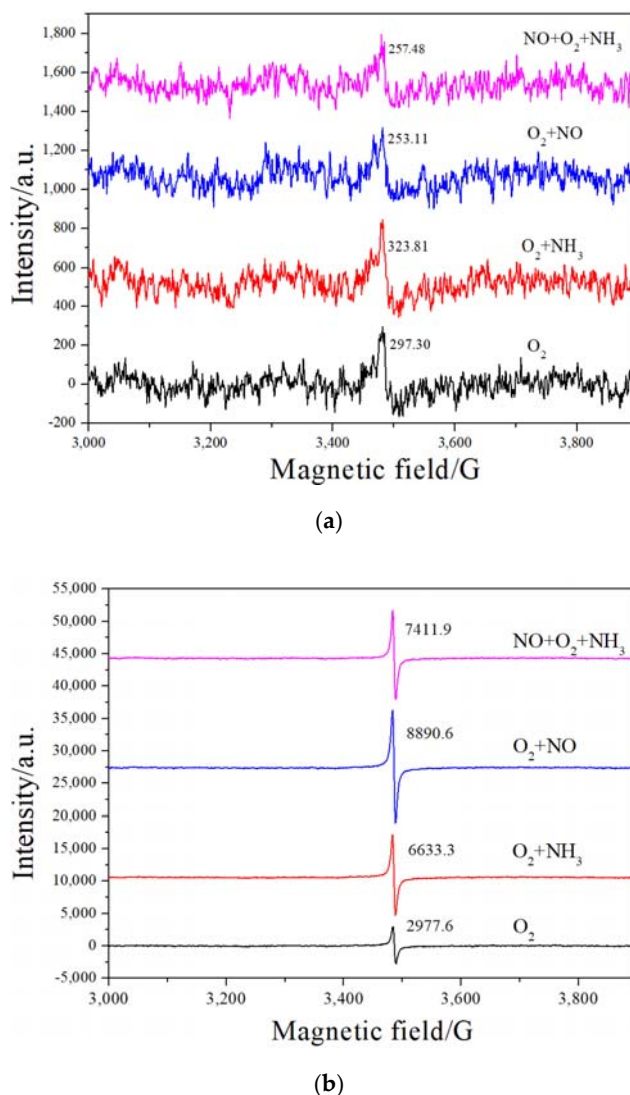
(a)

(b)

Figure 9. Electron paramagnetic resonance (EPR) spectra profiles of Ce/Ti-400 (**a**) and Ce-Ti-400 (**b**).

It also can be seen form Figure 9b that for the Ce-Ti-400 catalyst, the superoxide ion intensity of $NO + O_2$ test was higher than that of $NH_3 + O_2$. Therefore, similar to the NH_3 electron transfer mechanism, NO also could transfer electron to oxygen vacancies and produce superoxide ions. In addition, NO showed greater ability to transfer electron. It is worth noting that in the gas composition of $NO + O_2 + NH_3$, the superoxide ion intensity of Ce-Ti-400 decreased. In other words, only when NH_3, NO and O_2 co-existed would superoxide ions be consumed. From this phenomenon, the following inferences can be drawn: (1) It has been reported that superoxide ions could oxidize NO in SCR reaction [32] and this process would consume superoxide ions. However, compared to $NO + O_2 + NH_3$, superoxide ions signal of $NO + O_2$ was stronger. For low-temperature SCR reaction, NH_3 and NO adsorption took the leading role, exactly L-H mechanism [45]. Therefore, the reason for when NH_3, NO and O_2 co-existed the signal of superoxide ions decreased was that the reaction on activated NH_3 and NO with superoxide ions was much faster, which reflected the consumption of superoxide ions. (2) In the atmosphere of NH_3, NO and O_2, signal of superoxide ions still stronger than that in the atmosphere of O_2. For one thing, the adsorption of NO and NH_3 promoted the formation of superoxide ions; for another, the existence of superoxide ions would consume NO and NH_3 continually. Therefore, a favorable dynamic balance was formed in this process.

2.6. In Situ DRIFT (NH3 Adsorption after NO + O₂ Pre-Adsorption)

To further investigate the NO oxidation on the catalyst, In situ DRIFT was used in our experiment. Figure 10 showed the In situ DRIFT spectra of Ce/Ti-400 (a) and Ce-Ti-400 (b). Catalysts were pretreated in the atmosphere of 500 ppm NO + 5% O_2 at 240 °C. All curves were obtained by deducting the original catalyst signal. From Figure 10a, the spectra of Ce/Ti-400 showed little change after NO and O_2 were injected. From Figure 10b, we could find that a peak at 1621 cm^{-1} and 1603 cm^{-1} appeared immediately after NO and O_2 were injected. These peaks might be assigned to nitrate or nitrite. As time went on, the generation of other species was not found and the size of peak at 1621 cm^{-1} and 1603 cm^{-1} basically unchanged. Combined with the above experimental results, we could draw the following conclusions: Ce-Ti-400 could oxidize NO fast; the final product of NO was nitrate; the amount of nitrate from oxidation was stable. Therefore, Ce-Ti-400 showed stronger ability to oxidize NO than Ce/Ti-400, which could promote the SCR reaction at low temperature [46]. Combined with the discussion in this paper, we know that the increase of NO oxidation was related to the structure of Ce-□-Ti.
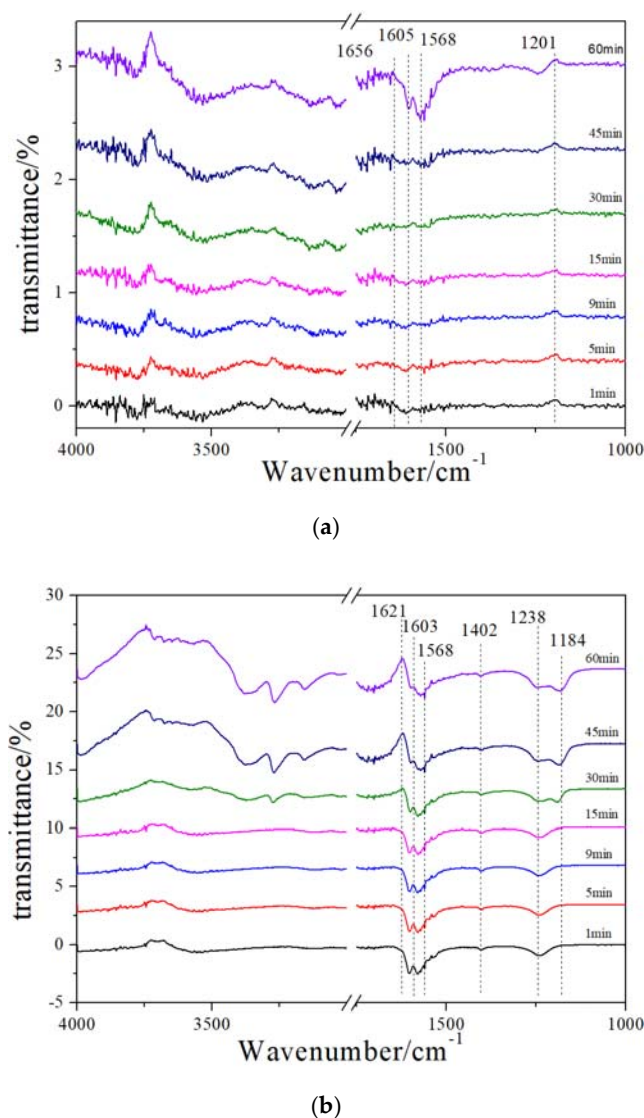

(a)

(b)

Figure 10. In situ DRIFT spectra of NH_3 reaction with pre-adsorbed. NO + O_2 over Ce/Ti-400 (**a**) and Ce-Ti-400 (**b**) at 240 °C.

3. Experimental

3.1. Synthesis of Catalysts

3.1.1. Synthesis of Doped Catalyst

Doped catalyst was synthesized by a sol-gel method. 1.19 g cerous nitrate was added to 20 mL of tetrabutyl titanate under continuous stirring. 80 mL ethanolic solution was added to dilute the solution. After stirring for 30 min, mixed solution of 20 mL ethanolic, 8 mL glacial acetic acid and 8 mL water was added in. Then the gel was aged under air for 2 days. After being heated at 120 °C for 6 h, the dried gel was calcined at 400 °C for 3 h. Doped catalyst calcined at different temperature was denoted as Ce-Ti-X (X represents the temperature of calcination). Catalyst without mixing cerium was donated as TiO_2.

3.1.2. Synthesis of Supported Catalyst

The preparation method of TiO_2 supporter was similar to the above without cerous nitrate. Then 3 g of supporter and 0.757 g cerous nitrate were added into 50 mL water under continuous stirring. After being heated at 60 °C for 4 h and dried at 120 °C for 6 h, the dried gel was calcined at 400 °C for 3 h. The supported catalyst calcined at different temperature was denoted as Ce/Ti-X (X represents the temperature of calcination).

3.2. Catalyst Activity Tests

The activity of different catalysts was carried out in a fixed-bed reactor (Quartz tube, inner diameter 5 mm). The temperature range was from 120 °C to 390 °C. 0.2 g catalyst sieving 60–80 mesh under normal pressure was used in this reaction. The reactant gas consisted of 500 ppm NO, 500 ppm NH_3, 5% O_2 and N_2 as a balance. The total flow rate was 500 mL/min. In addition, all the samples were kept on stream for 1 h to reach steady state at each temperature. The concentration of detected gas (NO, N_2O and O_2) in the inlet and outlet of the fixed-bed was measured by an in situ FT-IR gas analyzer (SERVOPRO 4900, Servomex, Sussex, UK). The NO conversion ratio could be calculated by the following equation:

$$\text{NO conversion (\%)} = ([NO]_{in} - [NO]_{out})/NO_{in} \times 100\%$$

3.3. Characterization

All the catalysts involved in this study were fresh catalysts, i.e., all kinds of catalysts were characterized immediately after calcination (catalysts for EPR were pretreatment at specific gas composition). The specific characterization was as follows: XRD patterns were collected at XD-3 diffractometer (Beijing Purkinje General Instrument Co., Ltd., (Beijing, China). Raman spectra were recorded with a Raman Spectrometer (Perkin-Elmer400F, PerkinElmer, Waltham, MA, USA). In situ DRIFTS experiments were carried out by a Nicolet IZ10 FTIR spectrometer (ThermoFisher, Waltham, MA, USA). XPS experiments were performed on a PHI-5000C ESCA system (PerkinElmer, Waltham, MA, USA) with Mg Kα radiation. Photoluminescence spectra (PL) were carried out on a Labram-HR800-type spectrophotometer (Jobin Yvon Co., Palaiseau, France). The EPR measurements were made with a Bruker EMX-10/12-type spectrometer in the X-band. Ammonia temperature-programmed desorption (NH_3-TPD), Nitric oxide temperature-programmed desorption (NO-TPD) and hydrogen temperature-programmed reduction (H_2-TPR) experiments were measured by a chemisorption analyzer (Quanta Chrome Instruments, Boynton Beach, FL, USA). Catalysts were pre-heated at 120 °C for 12 h before tests. About 0.3 g of catalyst was used. Experiments were carried out under a flow of He (70 mL·min^{-1}) for 1h at 400 °C. Subsequently, TPD was performed by ramping the temperature at 10 °C·min^{-1} in He (60 mL·min^{-1}). Then the NH_3 and NO adsorption was conducted under a flow rate of 70 mL·min^{-1} at room temperature. In the H_2-TPR experimental,

the sample was purged with 70 mL·min^{-1} He at 50 °C for 0.5 h and then heating the sample to 800 °C at a rate of 10 °C/min^{-1} after switched to a H$_2$/N$_2$ gas mixture (10% H$_2$, *v/v*) at a flow rate of 60 mL/min^{-1}.

4. Conclusions

Ce-Ti doped catalyst was synthesized by a sol-gel method and showed excellent NH$_3$-SCR activity, especially in the low-temperature range. Ce-Ti and Ce/Ti catalysts were characterized by XRD, Raman, XPS, PL, NO-TPD, NH$_3$-TPD, H$_2$-TPR, EPR and In situ DRIFT. The results revealed that structure of Ce-□-Ti existed in Ce-Txxi catalyst; oxygen vacancies on Ce-Ti catalyst promote the adsorption and activation of oxygen; oxygen was transferred to superoxide ions in large numbers. Ti and Ce sites were adsorption sites of NH$_3$ and NO, respectively, which transferred electrons to adsorbed oxygen and promoted the formation of superoxide ions. All of these were of great help for increasing the activity of SCR at low temperature.

References

1. Liu, G.; Gao, P.-X. A review of NOx storage/reduction catalysts: Mechanism, materials and degradation studies. *Catal. Sci. Technol.* **2011**, *1*, 552–568. [CrossRef]

2. Xie, X.; Lu, J.; Hums, E.; Huang, Q.; Lu, Z. Study on the Deactivation of V$_2$O$_5$-WO$_3$/TiO$_2$ Selective Catalytic Reduction Catalysts through Transient Kinetics. *Energy Fuels* **2015**, *29*, 3890–3896. [CrossRef]

3. Ding, S.; Liu, F.; Shi, X.; Liu, K.; Lian, Z.; Xie, L.; He, H. Significant Promotion Effect of Mo Additive on a Novel Ce-Zr Mixed Oxide Catalyst for the Selective Catalytic Reduction of NO$_{(x)}$ with NH$_3$. *ACS Appl. Mater. Interfaces* **2015**, *7*, 9497–9506. [CrossRef] [PubMed]

4. Qi, G.; Yang, R.T.; Chang, R. MnO$_x$-CeO$_2$ mixed oxides prepared by co-precipitation for selective catalytic reduction of NO with NH$_3$ at low temperatures. *Appl. Catal. B Environ.* **2004**, *51*, 93–106. [CrossRef]

5. Contreras-García, M.E.; García-Benjume, M.L.; Macías-Andrés, V.I.; Barajas-Ledesma, E.; Medina-Flores, A.; Espitia-Cabrera, M.I. Synergic effect of the TiO$_2$-CeO$_2$ nanoconjugate system on the band-gap for visible light photocatalysis. *Mater. Sci. Eng. B* **2014**, *183*, 78–85. [CrossRef]

6. Muñoz-Batista, M.J.; Gómez-Cerezo, M.N.; Kubacka, A.; Tudela, D.; Fernández-García, M. Role of Interface Contact in CeO$_2$–TiO$_2$ Photocatalytic Composite Materials. *ACS Catal.* **2013**, *4*, 63–72. [CrossRef]

7. Zhang, R.; Zhong, Q.; Zhao, W.; Yu, L.; Qu, H. Promotional effect of fluorine on the selective catalytic reduction of NO with NH$_3$ over CeO$_2$-TiO$_2$ catalyst at low temperature. *Appl. Surface Sci.* **2014**, *289*, 237–244. [CrossRef]

8. Gao, X.; Jiang, Y.; Zhong, Y.; Luo, Z.; Cen, K. The activity and characterization of CeO$_2$-TiO$_2$ catalysts prepared by the sol-gel method for selective catalytic reduction of NO with NH$_3$. *J. Hazard. Mater.* **2010**, *174*, 734–739. [CrossRef] [PubMed]

9. Li, P.; Xin, Y.; Li, Q.; Wang, Z.; Zhang, Z.; Zheng, L. Ce-Ti amorphous oxides for selective catalytic reduction of NO with NH$_3$: Confirmation of Ce-O-Ti active sites. *Environ. Sci. Technol.* **2012**, *46*, 9600–9605. [CrossRef] [PubMed]

10. Li, Q.; Gu, H.; Li, P.; Zhou, Y.; Liu, Y.; Qi, Z.; Xin, Y.; Zhang, Z. In situ IR studies of selective catalytic reduction of NO with NH$_3$ on Ce-Ti amorphous oxides. *Chin. J. Catal.* **2014**, *35*, 1289–1298. [CrossRef]

11. Mosrati, J.; Atia, H.; Eckelt, R.; Lund, H.; Agostini, G.; Bentrup, U.; Rockstroh, N.; Keller, S.; Armbruster, U.; Mhamdi, M. Nb-Modified Ce/Ti Oxide Catalyst for the Selective Catalytic Reduction of NO with NH$_3$ at Low Temperature. *Catalysts* **2018**, *8*, 175. [CrossRef]

12. Liu, Z.; Liu, H.; Feng, X.; Ma, L.; Cao, X.; Wang, B. Ni-Ce-Ti as a superior catalyst for the selective catalytic reduction of NO_x with NH_3. *J. Mol. Catal.* **2018**, *445*, 179–186. [CrossRef]

13. Zhao, W.; Tang, Y.; Wan, Y.; Li, L.; Yao, S.; Li, X. Promotion effects of SiO_2 or/and Al_2O_3 doped CeO_2/TiO_2 catalysts for selective catalytic reduction of NO by NH_3. *J. Hazard. Mater.* **2014**, *278*, 350–359. [CrossRef] [PubMed]

14. Liu, Z.; Liu, H.; Zeng, H.; Xu, Q. A novel Ce–Sb binary oxide catalyst for the selective catalytic reduction of NO_x with NH_3. *Catal. Sci. Technol.* **2016**, *6*, 8063–8071. [CrossRef]

15. Zhang, Y.; Yuwono, A.H.; Wang, J.; Li, J. Enhanced Photocatalysis by Doping Cerium into Mesoporous Titania Thin Films. *J. Phys. Chem. C* **2009**, *113*, 21406–21412. [CrossRef]

16. Kityakarn, S.; Worayingyong, A.; Suramitr, A.; Smith, M.F. Ce-doped nanoparticles of TiO_2: Rutile-to-brookite phase transition and evolution of Ce local-structure studied with XRD and XANES. *Mater. Chem. Phys.* **2013**, *139*, 543–549. [CrossRef]

17. Mateos-Pedrero, C.; González-Carrazán, S.R.; Soria, M.A.; Ruíz, P. Effect of the nature of TiO_2 support over the performances of Rh/TiO_2 catalysts in the partial oxidation of methane. *Catal. Today* **2013**, *203*, 158–162. [CrossRef]

18. Liu, B.; Zhao, X.; Zhang, N.; Zhao, Q.; He, X.; Feng, J. Photocatalytic mechanism of TiO_2–CeO_2 films prepared by magnetron sputtering under UV and visible light. *Surf. Sci.* **2005**, *595*, 203–211. [CrossRef]

19. Liu, Z.; Yi, Y.; Li, J.; Woo, S.I.; Wang, B.; Cao, X.; Li, Z. A superior catalyst with dual redox cycles for the selective reduction of $NO_{(x)}$ by ammonia. *Chem. Commun.* **2013**, *49*, 7726–7728. [CrossRef] [PubMed]

20. Shang, D.; Zhong, Q.; Cai, W. High performance of NO oxidation over Ce–Co–Ti catalyst: The interaction between Ce and Co. *Appl. Surf. Sci.* **2015**, *325*, 211–216. [CrossRef]

21. Liotta, L.F.; Di Carlo, G.; Pantaleo, G.; Venezia, A.M.; Deganello, G. Co_3O_4/CeO_2 composite oxides for methane emissions abatement: Relationship between Co_3O_4–CeO_2 interaction and catalytic activity. *Appl. Catal. B Environ.* **2006**, *66*, 217–227. [CrossRef]

22. Nasir, M.; Xi, Z.; Xing, M.; Zhang, J.; Chen, F.; Tian, B.; Bagwasi, S. Study of Synergistic Effect of Ce- and S-Codoping on the Enhancement of Visible-Light Photocatalytic Activity of TiO_2. *J. Phys. Chem. C* **2013**, *117*, 9520–9528. [CrossRef]

23. Liu, J.; Han, R.; Zhao, Y.; Wang, H.; Lu, W.; Yu, T.; Zhang, Y. Enhanced Photoactivity of V−N Codoped TiO_2 Derived from a Two-Step Hydrothermal Procedure for the Degradation of PCP−Na under Visible Light Irradiation. *J. Phys. Chem. C* **2011**, *115*, 4507–4515. [CrossRef]

24. Wang, Y.; Wang, Y.; Meng, Y.; Ding, H.; Shan, Y.; Zhao, X.; Tang, X. A Highly Efficient Visible-Light-Activated Photocatalyst Based on Bismuth- and Sulfur-Codoped TiO_2. *J. Phys. Chem. C* **2008**, *112*, 6620–6626. [CrossRef]

25. Zhao, L.; Park, S.G.; Magyari-Köpe, B.; Nishi, Y. First principles modeling of charged oxygen vacancy filaments in reduced TiO_2 –implications to the operation of non-volatile memory devices. *Math. Comput. Model.* **2013**, *58*, 275–281. [CrossRef]

26. Li, D.; Haneda, H.; Labhsetwar, N.K.; Hishita, S.; Ohashi, N. Visible-light-driven photocatalysis on fluorine-doped TiO_2 powders by the creation of surface oxygen vacancies. *Chem. Phys. Lett.* **2005**, *401*, 579–584. [CrossRef]

27. Li, D.; Ohashi, N.; Hishita, S.; Kolodiazhnyi, T.; Haneda, H. Origin of visible-light-driven photocatalysis: A comparative study on N/F-doped and N–F-codoped TiO_2 powders by means of experimental characterizations and theoretical calculations. *J. Solid State Chem.* **2005**, *178*, 3293–3302. [CrossRef]

28. Yu, L.; Zhong, Q.; Deng, Z.; Zhang, S. Enhanced NO_x removal performance of amorphous Ce-Ti catalyst by hydrogen pretreatment. *J. Mol. Catal. A Chem.* **2016**, *423*, 371–378. [CrossRef]

29. Li, H.; Zhang, S.; Zhong, Q. Effect of nitrogen doping on oxygen vacancies of titanium dioxide supported vanadium pentoxide for ammonia-SCR reaction at low temperature. *J. Colloid Interface Sci.* **2013**, *402*, 190. [CrossRef] [PubMed]

30. Funk, S.; Hokkanen, B.; Burghaus, U.; Ghicov, A.; Schmuki, P. Unexpected adsorption of oxygen on TiO2 nanotube arrays: Influence of crystal structure. *Nano Lett.* **2007**, *7*, 1091–1094. [CrossRef] [PubMed]

31. Meng, D.; Zhan, W.; Guo, Y.; Guo, Y.; Wang, L.; Lu, G. A highly effective catalyst of Sm-MnO_x for the NH_3-SCR of NO_x at low temperature: The promotional role of Sm and its catalytic performance. *ACS Catal.* **2015**, *5*, 5973–5983. [CrossRef]

32. Zhang, S.; Zhong, Q.; Zhao, W.; Li, Y. Surface characterization studies on F-doped V_2O_5/TiO_2 catalyst for NO reduction with NH 3 at low-temperature. *Chem. Eng. J.* **2014**, *253*, 207–216. [CrossRef]

33. Ballinger, T.H.; Yates, J.T. IR spectroscopic detection of Lewis acid sites on alumina using adsorbed carbon monoxide. Correlation with aluminum-hydroxyl group removal. *Langmuir* **1991**, *7*, 3041–3045. [CrossRef]

34. Jiang, Y.; Xing, Z.; Wang, X.; Huang, S.; Wang, X.; Liu, Q. Activity and characterization of a Ce–W–Ti oxide catalyst prepared by a single step sol-gel method for selective catalytic reduction of NO with NH_3. *Fuel* **2015**, *151*, 124–129. [CrossRef]

35. Chen, H.; Sayari, A.; Adnot, A.; Larachi, F.C. Composition–activity effects of Mn-Ce-O composites on phenol catalytic wet oxidation. *Appl. Catal. B* **2001**, *32*, 195–204. [CrossRef]

36. Inturi, S.N.R.; Boningari, T.; Suidan, M.; Smirniotis, P.G. Visible-light-induced photodegradation of gas phase acetonitrile using aerosol-made transition metal (V, Cr, Fe, Co, Mn, Mo, Ni, Cu, Y, Ce, and Zr) doped TiO_2. *Appl. Catal. B* **2014**, *144*, 333–342. [CrossRef]

37. Dall'acqua, L.; Nova, I.; Lietti, L.; Ramis, G.; Busca, G.; Giamello, E. Spectroscopic characterisation of MoO_3/TiO_2 deNO$_x$-SCR catalysts: Redox and coordination properties. *Phys. Chem. Chem. Phys.* **2000**, *2*, 4991–4998. [CrossRef]

38. Chen, Y.; Cao, X.; Lin, B.; Gao, B. Origin of the visible-light photoactivity of NH_3-treated TiO_2: Effect of nitrogen doping and oxygen vacancies. *Appl Surf. Sci.* **2013**, *264*, 845–852. [CrossRef]

39. Wang, Y.; Ge, C.Z.; Zhan, L.; Li, C.; Qiao, W.; Ling, L. MnO$_x$-CeO$_2$/Activated Carbon Honeycomb Catalyst for Selective Catalytic Reduction of NO with NH_3 at Low Temperatures. *Ind. Eng. Chem. Res.* **2012**, *51*, 11667–11673. [CrossRef]

40. Yao, X.; Zhao, R.; Chen, L.; Du, J.; Tao, C.; Yang, F. Selective catalytic reduction of NO$_x$ by NH_3 over CeO_2 supported on TiO_2: Comparison of anatase, brookite, and rutile. *Appl. Catal. B Environ.* **2017**, *208*, 82–93. [CrossRef]

41. Wang, C.; Yang, S.; Chang, H.; Peng, Y.; Li, J. Dispersion of tungsten oxide on SCR performance of $V_2O_5WO_3/TiO_2$: Acidity, surface species and catalytic activity. *Chem. Eng. J.* **2013**, *225*, 520–527. [CrossRef]

42. Mu, W.; Zhu, J.; Zhang, S.; Guo, Y.; Su, L.; Li, X.; Li, Z. Novel proposition on mechanism aspects over Fe-Mn/ZSM-5 catalyst for NH_3-SCR of NO$_x$ at low temperature: Rate and direction of multifunctional electron-transfer-bridge and in-situ DRIFTs analysis. *Catal. Sci. Technol.* **2016**. [CrossRef]

43. Volodin, A.M.; Cherkashin, A.E.; Zakharenko, V.S. Influence of physically adsorbed oxygen on the separation of electron-hole pairs on anatase irradiated by visible light. *React. Kinet. Catal. Lett.* **1979**, *11*, 103–106. [CrossRef]

44. Volodin, A.M.; Cherkashin, A.E.; Zakharenko, V.S. Formation of O_2^- ion-radicals on reduced anatase. Influence of adsorbed CO on the stabilization of O_2^-. *React. Kinet. Catal. Lett.* **1979**, *11*, 107–111. [CrossRef]

45. Chen, L.; Li, J.; Ge, M. DRIFT study on cerium-tungsten/titania catalyst for selective catalytic reduction of NO$_x$ with NH_3. *Environ. Sci. Technol.* **2010**, *44*, 9590. [CrossRef] [PubMed]

46. Ellmers, I.; Vélez, R.P.; Bentrup, U.; Schwieger, W.; Brückner, A.; Grünert, W. SCR and NO oxidation over Fe-ZSM-5—The influence of the Fe content. *Catal. Today* **2015**, *258*, 337–346. [CrossRef]